

# Lyapunov control-inspired strategies for quantum combinatorial optimization

Alicia B. Magann,<sup>1,2</sup> Kenneth M. Rudinger,<sup>3</sup> Matthew D. Grace,<sup>1</sup> and Mohan Sarovar<sup>1</sup>

<sup>1</sup>*Extreme-Scale Data Science & Analytics, Sandia National Laboratories, Livermore, California 94550, USA*

<sup>2</sup>*Department of Chemical & Biological Engineering,*

*Princeton University, Princeton, New Jersey 08544, USA*

<sup>3</sup>*Center for Computing Research, Sandia National Laboratories, Albuquerque, New Mexico 87185, USA*

(Dated: August 21, 2021)

The prospect of using quantum computers to solve combinatorial optimization problems via the quantum approximate optimization algorithm (QAOA) has attracted considerable interest in recent years. However, a key limitation associated with QAOA is the need to classically optimize over a set of quantum circuit parameters. This classical optimization can have significant associated costs and challenges. Here, we provide an expanded description of Lyapunov control-inspired strategies for quantum optimization, as first presented in [arXiv:2103.08619](https://arxiv.org/abs/2103.08619), that do not require any classical optimization effort. Instead, these strategies utilize feedback from qubit measurements to assign values to the quantum circuit parameters in a deterministic manner, such that the combinatorial optimization problem solution improves monotonically with the quantum circuit depth. Numerical analyses are presented that investigate the utility of these strategies towards MaxCut on weighted and unweighted 3-regular graphs, both in ideal implementations and also in the presence of measurement noise. We also discuss how these strategies may be used to seed QAOA optimizations in order to improve performance for near-term applications, and explore connections to quantum annealing.

## I. INTRODUCTION

Combinatorial optimization problems have broad and high-value applications, including in logistics and supply chain optimization. The desire to use quantum resources to aid in solving them has a long history, spanning the development of adiabatic and annealing-based strategies [1–3], as well as the development of early quantum algorithms [4, 5]. More recently, the quantum approximate optimization algorithm (QAOA) [6] was proposed in 2014, as a method for leveraging quantum computers to solve combinatorial optimization problems. In particular, QAOA is a method for determining an approximate solution to a combinatorial optimization problem by encoding the associated cost function  $C$  into an Ising Hamiltonian  $H_p$ , such that the solution of the combinatorial optimization problem is encoded in the ground state of  $H_p$ . Then, QAOA operates in a hybrid quantum-classical framework; a classical computer is utilized to iteratively minimize the value of  $\langle \psi(\{\gamma_k\}, \{\beta_k\}) | H_p | \psi(\{\gamma_k\}, \{\beta_k\}) \rangle$  over the set of  $2\ell$  parameters  $\{\gamma_k\}_{k=1}^\ell$  and  $\{\beta\}_{k=1}^\ell$ . Meanwhile, a quantum computer is utilized to prepare the parametrized, multiqubit state  $|\psi(\{\gamma_k\}, \{\beta_k\})\rangle$ , by using a parameterized quantum circuit of the form  $U_{QAOA} = U_d(\beta_\ell)U_p(\gamma_\ell) \cdots U_d(\beta_1)U_p(\gamma_1)$ , such that  $|\psi(\{\gamma_k\}, \{\beta_k\})\rangle = U_{QAOA}|\psi_0\rangle$ . The elements of the circuit,  $U_p(\cdot)$  and  $U_d(\cdot)$ , are created by evolution of the system under  $H_p$  and under a *driver* Hamiltonian  $H_d$ , which is chosen to not commute with  $H_p$ . Since its development, QAOA has captured the attention of numerous theoretical and experimental groups, e.g., [7–12], particularly as a potential application of noisy, intermediate-scale quantum (NISQ) [13] devices.

Recently, numerous connections have been made between QAOA and quantum optimal control (QOC) [14],

which is a strategy for identifying the controls needed to steer the dynamics of a quantum system in a desired manner by iteratively optimizing over a set of control functions or parameters [15, 16]. Certain connections have rested on the control-theoretic notion of controllability, which implies that QOC solutions can be found for driving the dynamics of a system under consideration towards arbitrary objectives [17–24]. For instance, controllability considerations have recently been applied to show that QAOA can be computationally universal in certain circumstances [25, 26], and to assess the number of QAOA quantum circuit parameters needed to achieve controllability [27]. Tools from QOC have also been used to show that under certain assumptions, a bang-bang approach akin to QAOA is optimal for minimizing the expectation value of  $H_p$  [28]. It has also been shown that bang-bang QOC protocols like QAOA can yield exponential speedups in certain problem settings, compared with quasistatic scheduling [29]. A more recent analysis has subsequently shown that optimal QAOA solutions can be more generally described by bang-anneal-bang schedules [30].

A key challenge in identifying QAOA and QOC solutions is the difficulty of searching for the optimal QAOA and QOC parameters, respectively. If the number of QAOA layers, and correspondingly variational parameters, can be limited to  $O(\text{poly}(\log(n)))$ , then the complexity scaling of the optimization can be polynomial in  $n$ . However, this scaling belies the difficulty of such optimizations – the fact is that QAOA, and most variational algorithms, require optimization over non-linear, stochastic cost functions with derivative information that is noisy and hard to obtain. Scaling classical optimization to thousands of parameters is challenging in this context, e.g., [31].

Even in the absence of noise, the difficulty of identifying the optimal parameters is determined in large part by the structure of the optimization landscape, and landscape features such as local optima, saddle points, and barren plateaus can complicate and hinder the optimization process [32–39]. However, we note that a variety of alternate quantum control frameworks, including quantum tracking control [40–44], quantum Lyapunov control [45–53], and quantum feedback control [54–57], have been developed that do not rely on the iterative classical optimization procedure inherent to QOC and thus do not share these challenges.

Here, we explore a new connection between quantum algorithms and quantum control theory, and develop strategies for quantum combinatorial optimization inspired by the theory of *quantum Lyapunov control* (QLC). In particular, this article provides an expanded discussion of the details of these strategies, beyond that contained in [58]. Importantly, these QLC-inspired strategies do not involve any classical optimization. Instead, they use measurement-based feedback to assign values to the quantum circuit parameters. We show that this feedback-based procedure yields a monotonically improving solution to the original combinatorial optimization problem, with respect to the depth of the quantum circuit.

The remainder of this article is organized as follows. We begin by describing certain aspects of QLC. We then introduce a Feedback-based ALgorithm for Quantum OptimizatioN (FALQON) inspired by this QLC framework, and discuss extensions that can be used to improve performance, including the addition of a reference perturbation, the implementation of an iterative procedure, and the introduction of additional control functions. We then discuss applications of FALQON towards solving the MaxCut problem. To this end, we provide numerical illustrations of the ideal performance of FALQON towards solving MaxCut on 3-regular graphs, and we also explore how it performs in the presence of measurement noise. We go on to discuss how FALQON can be used to boost the performance of QAOA in NISQ applications, and explore connections to quantum annealing. We conclude with an outlook.

## II. QUANTUM LYAPUNOV CONTROL

Quantum Lyapunov control (QLC) is a local-in-time method for identifying controls to asymptotically steer the dynamics of a quantum system towards a desired objective [45–53]. The controls are identified utilizing a feedback law, which is derived from a suitable control Lyapunov function [59], chosen to capture the target objective. In this section, we describe the theory of QLC and outline certain results from the literature pertaining to its asymptotic convergence behavior. We begin by considering a quantum system whose dynamics are

governed by

$$i \frac{d}{dt} |\psi(t)\rangle = (H_p + H_d \beta(t)) |\psi(t)\rangle \quad (1)$$

where  $H_p$  is the *drift* Hamiltonian and  $H_d$  is the *control* Hamiltonian that couples a scalar, time-dependent control function  $\beta(t)$  to the system. In this article, we choose our QLC objective to be the minimization of  $\langle H_p \rangle = \langle \psi(t) | H_p | \psi(t) \rangle$ , and thus seek a QLC strategy for designing  $\beta(t)$  to accomplish this. We proceed by defining a Lyapunov function

$$E_p(|\psi(t)\rangle) = \langle \psi(t) | H_p | \psi(t) \rangle \quad (2)$$

to capture our QLC objective. Then, to minimize  $E_p$  we seek to design  $\beta(t)$  such that the QLC condition

$$\frac{d}{dt} E_p \leq 0, \quad \forall t \geq 0 \quad (3)$$

is satisfied. There is significant flexibility in choosing  $\beta(t)$  to satisfy Eq. (3). Namely, given that

$$\begin{aligned} \frac{dE_p}{dt} &= \langle \psi(t) | i[H_p + \beta(t)H_d, H_p] | \psi(t) \rangle \\ &= \langle \psi(t) | i[\beta(t)H_d, H_p] | \psi(t) \rangle \\ &= \langle \psi(t) | i[H_d, H_p] | \psi(t) \rangle \beta(t) \\ &= A(t) \beta(t), \end{aligned} \quad (4)$$

where

$$A(t) \equiv \langle \psi(t) | i[H_d, H_p] | \psi(t) \rangle, \quad (5)$$

we may take

$$\beta(t) = -w f(t, A(t)), \quad (6)$$

for  $w > 0$ , where  $f(t, A(t))$  is any continuous function with  $f(t, 0) = 0$  and  $A(t)f(t, A(t)) > 0$  for all  $A(t) \neq 0$  [60]. This choice of  $\beta(t)$  guarantees that  $E_p$  will decrease monotonically over time. When  $\beta(t)$  is chosen according to Eq. (6), the system dynamics are governed by

$$i \frac{d}{dt} |\psi(t)\rangle = (H_p + H_d \beta(t, A(t))) |\psi(t)\rangle, \quad (7)$$

which are highly nonlinear, due to the dependence of  $\beta(t)$  on the state  $|\psi(t)\rangle$  via  $A(t)$ .

We refer to Eq. (6) as a *feedback law*, as it relies on feedback in order to evaluate the observable expectation value  $A(t)$ . Conventionally, QLC laws like Eq. (6) are used in simulations to design open-loop control laws; that is, they cannot be applied directly in experiments as-is, as the destructive, real-time measurements required to estimate  $A(t)$  would lead to a collapse of the system state. This distinguishes QLC from real-time feedback control.

Ideally, designing  $\beta$  per Eq. (6) would result in asymptotic convergence to the global minimum of  $E_p$ , and it has been shown that this behavior can be guaranteed when

a set of sufficient conditions are met [51, 60–62]. However, these conditions are very stringent (see Appendix A). When the protocol we construct in Sec. III is applied to the MaxCut problem, per Sec. IV, they are not satisfied. Nonetheless, asymptotic convergence to the global minimum can still be obtained in such settings (e.g., as illustrated in Fig. 1), and in situations where convergence is not obtained, a variety of techniques can be employed to improve control performance, as discussed in the following subsections.

### A. Inclusion of reference perturbation in $\beta(t)$

The inclusion of a reference perturbation in  $\beta(t)$  can improve the likelihood of asymptotic convergence to the global minimum of  $E_p$  [60–62]. Here, we consider the inclusion of a reference perturbation  $\lambda(t)$  such that the time-dependent system Hamiltonian is given by

$$H(t) = H_p + (\lambda(t) + \beta(t))H_d. \quad (8)$$

Inspecting Eq. (8), we may define system (a) as a system with drift Hamiltonian  $H_p$ , control Hamiltonian  $H_d$ , and control function  $(\lambda(t) + \beta(t))$ . Meanwhile, we may define system (b) as a perturbed system with time-dependent drift Hamiltonian

$$H_{p,(b)}(t) \equiv H_p + \lambda(t)H_d, \quad (9)$$

control Hamiltonian  $H_d$ , and control function  $\beta(t)$ . Within (b), we may define the perturbed Lyapunov function

$$E_{p,(b)}(|\psi(t)\rangle) = \langle\psi(t)|H_{p,(b)}(t)|\psi(t)\rangle, \quad (10)$$

and seek a control law that will ensure

$$\frac{dE_{p,(b)}}{dt} \leq 0, \quad (11)$$

while at the same time, ideally improving convergence to the minimum of our original objective  $E_p$ . At this stage, it is important to note that in practice,  $\lambda(t)$  can be defined explicitly as a desired function of  $t$ , or implicitly as a function of  $|\psi(t)\rangle$ ,  $E_p$ , or  $E_{p,(b)}$ . For practical reasons, we restrict our attention to the former case; for further details on the latter, we refer to refs. [61, 62].

When  $\lambda(t)$  is defined as an explicit function of time, the left-side of Eq. (11) is given, conveniently, by,

$$\begin{aligned} \frac{d}{dt}E_{p,(b)} &= \langle\psi(t)|i[H(t), H_{p,(b)}(t)]|\psi(t)\rangle \\ &= \langle\psi(t)|i[H_{p,(b)}(t) + \beta(t)H_d, H_{p,(b)}(t)]|\psi(t)\rangle \\ &= \langle\psi(t)|i[\beta(t)H_d, H_{p,(b)}(t)]|\psi(t)\rangle \\ &= \langle\psi(t)|i[H_d, H_p]|\psi(t)\rangle\beta(t) \\ &= A(t)\beta(t) \end{aligned} \quad (12)$$

which implies that even after the inclusion of the reference perturbation  $\lambda(t)$  and the definition of a perturbed

Lyapunov function  $E_{p,(b)}$ , we may nonetheless define the control law for  $\beta(t)$  as before, as  $\beta(t) = -w f(t, A(t))$ , to ensure Eq. (11) is satisfied.

Within this framework, if system (b) converges to the ground state of  $H_{p,(b)}(t)$  at a terminal time  $t = T$ , and  $\lambda(T) = 0$ , then system (b) becomes system (a), such that  $H_{p,(b)}(T) = H_p$ , meaning that the ground state of  $H_{p,(b)}(t)$  is also the ground state of  $H_p$ , and convergence to the desired state has been obtained. As such, it is often practical to select  $\lambda(t)$  to be a slowly-varying function that tends to 0 as  $t \rightarrow T$ .

### B. Iterative quantum Lyapunov control

Another technique to improve the likelihood of asymptotic convergence to the minimum of  $E_p$  is to use an iterative procedure for refining the QLC control function  $\beta(t)$  [52]. We emphasize that the iterative QLC procedure outlined in this section is conceptually distinct from the iterative optimization procedure utilized in QOC, as the iterations involved do not involve updates determined by an optimization routine. Instead,  $\beta(t)$  is updated using a QLC-derived control law, in the following manner.

We begin by considering a system initialized as  $|\psi(t=0)\rangle = |\psi_0\rangle$ , and then design a control field  $\beta^{(0)}(t)$  to control  $E_p$  using QLC, as per the control law of Eq. (6), over some fixed time interval  $t \in [0, T]$ . We denote the trajectory of  $E_p$  over this time interval by  $E_p^{(0)}(t)$ , and denote the associated state by  $|\psi^{(0)}(t)\rangle$ . Subsequent steps are then carried out as follows. For iterations  $j \geq 1$ ,  $\beta^{(j-1)}(t)$  serves as a reference perturbation, as denoted by  $\lambda(t)$  in Sec. II A. Then,  $\beta^{(j-1)}(t)$ ,  $E_p^{(j-1)}(t)$ , and  $|\psi^{(j-1)}(t)\rangle$  all describe the dynamics of a perturbed system (b), whose time-dependent Hamiltonian is

$$H_{p,(b)}^{(j-1)}(t) = H_p + \beta^{(j-1)}(t)H_d. \quad (13)$$

A new QLC field  $\tilde{\beta}^{(j)}(t)$  is then determined for  $t \in [0, T]$  using the framework in Sec. II A, where a perturbed Lyapunov function based on  $H_{p,(b)}^{(j-1)}$  is utilized, and  $\tilde{\beta}^{(j)}(t)$  is chosen according to Eq. (6). After  $\tilde{\beta}^{(j)}(t)$  has been computed for  $t \in [0, T]$ , the update rule is given by

$$\beta^{(j)}(t) = \beta^{(j-1)}(t) + \tilde{\beta}^{(j)}(t). \quad (14)$$

For  $T$  chosen to be large enough for the perturbed system to converge to the unperturbed system at each iteration, i.e., such that  $\beta^{(j)}(T) = 0$ , causing  $H_{p,(b)}^{(j)}(T) = H_p$ ,  $\forall j$ , this procedure guarantees a monotonic improvement

of  $E_p(T)$  with respect to iteration, as per,

$$\begin{aligned}
\langle \psi^{(j)}(T) | H_p | \psi^{(j)}(T) \rangle &= \langle \psi^{(j)}(T) | H_{p,(b)}^{(j-1)}(T) | \psi^{(j)}(T) \rangle \\
&\leq \langle \psi^{(j)}(0) | H_{p,(b)}^{(j-1)}(0) | \psi^{(j)}(0) \rangle \\
&= \langle \psi_0 | H_{p,(b)}^{(j-1)}(0) | \psi_0 \rangle \\
&= \langle \psi^{(j-1)}(0) | H_{p,(b)}^{(j-1)}(0) | \psi^{(j-1)}(0) \rangle \\
&= \langle \psi^{(j-1)}(T) | H_{p,(b)}^{(j-1)}(T) | \psi^{(j-1)}(T) \rangle \\
&= \langle \psi^{(j-1)}(T) | H_p | \psi^{(j-1)}(T) \rangle,
\end{aligned} \tag{15}$$

such that  $E_p^{(j)}(T) \leq E_p^{(j-1)}(T)$  [52]. We note that in line 5 of the above, we have utilized the fact that  $\frac{d}{dt} \langle \psi^{(j-1)}(t) | H_{p,(b)}^{(j-1)}(t) | \psi^{(j-1)}(t) \rangle = 0$ , due to the fact that  $|\psi^{(j-1)}(t)\rangle$  evolves under  $H_{p,(b)}^{(j-1)}(t)$ .

### C. Extensions to multiple control functions

The framework of QLC can be extended in a straightforward manner to settings with multiple control functions, i.e., where the system Hamiltonian is given by

$$H(t) = H_p + \sum_j \beta(j, t) H_{d,j}, \tag{16}$$

where  $\beta(j, t)$  denotes the value of the control function that scales the  $j$ -th control Hamiltonian  $H_{d,j}$  at time  $t$ . Then, in order to satisfy the QLC condition that  $\frac{d}{dt} E_p \leq 0$ , we see that

$$\begin{aligned}
\frac{d}{dt} \langle \psi(t) | H_p | \psi(t) \rangle &= \langle \psi(t) | i[H_p + \sum_j \beta(j, t) H_{d,j}, H_p] | \psi(t) \rangle \\
&= \langle \psi(t) | i[\sum_j \beta(j, t) H_{d,j}, H_p] | \psi(t) \rangle \\
&= \sum_j \langle \psi(t) | i[H_{d,j}, H_p] | \psi(t) \rangle \beta(j, t) \\
&= \sum_j A(j, t) \beta(j, t),
\end{aligned} \tag{17}$$

where

$$A(j, t) \equiv \langle \psi(t) | i[H_{d,j}, H_p] | \psi(t) \rangle. \tag{18}$$

As such, the following control laws may be used:

$$\beta(j, t) = -w_j f_j(t, A(j, t)), \quad \forall j \tag{19}$$

to ensure that  $E_p$  decreases monotonically over time. We remark that in cases with multiple control functions, reference perturbations may be included for any  $\beta(j, t)$ , following the framework outlined in Sec. II A, and iterative QLC schemes can also be used, following the framework of Sec. II B.

## III. FEEDBACK-BASED ALGORITHM FOR QUANTUM OPTIMIZATION

We now consider how the QLC framework outlined in Sec. II (eqs. (3) – (6)) can be translated into FALQON, a feedback-based algorithm for minimizing the expectation value of a Hamiltonian, that can be implemented on quantum devices. To this end, we now assume that  $H_p$  is the problem Hamiltonian that encodes a combinatorial optimization problem of interest, noting that when defined this way,

$$E_p = \langle \psi(t) | H_p | \psi(t) \rangle \tag{20}$$

may not meet all of the requirements of being a true Lyapunov function, such as positive definiteness. Now, without loss of generality, we consider alternating, rather than concurrent, applications of  $H_p$  and  $H_d$ , such that the state  $|\psi(t)\rangle$  undergoes a time evolution of the form

$$U = U_d(\beta_\ell) U_p \cdots U_d(\beta_1) U_p, \tag{21}$$

where

$$U_p \equiv e^{-iH_p \Delta t} \tag{22}$$

and

$$U_d(\beta_k) \equiv e^{-i\beta_k H_d \Delta t} \tag{23}$$

and  $\beta_k = \beta(2k\Delta t)$  for  $k = 1, 2, \dots, \ell$ , such that after each period of  $\Delta t$ , the Hamiltonian that is applied alternates between  $H_p$  and  $H_d$ . For small  $\Delta t$ , this yields a Trotterized approximation to the time evolution that would be achieved in Eq. (1). To ensure that Eq. (3) is satisfied, we may again define  $\beta$  from Eq. (6). In this work, we use

$$w = 1, \quad f(t, A(t)) = A(t), \tag{24}$$

such that in the alternating framework

$$\beta_{k+1} = -A_k, \tag{25}$$

where  $A_k = \langle \psi_k | i[H_d, H_p] | \psi_k \rangle$ , and  $|\psi_k\rangle = |\psi(2k\Delta t)\rangle$ . Importantly, we note that it is always possible to select  $\Delta t$  small enough such that Eq. (3) is satisfied when the control law in Eq. (25) is used (see Sec. III A). However, if  $\Delta t$  is chosen to be too large, the condition in Eq. (3) can be violated.

The implementation of this alternating procedure on a qubit device can be accomplished according to the steps in Algorithm 1. The preliminary step is to seed the procedure by setting  $\beta_1 = \beta_{\text{init}}$ , and we use  $\beta_{\text{init}} = 0$ . Then, a set of qubits are initialized in a fixed initial state  $|\psi_0\rangle$ , and a single “layer” is implemented to prepare the state

$$|\psi_1\rangle = U_d(\beta_1) U_p |\psi_0\rangle. \tag{26}$$

Next, the qubits are then measured in order to estimate  $A_1$ . This can be accomplished by expanding  $A_1$  in the

Pauli operator basis as

$$A_1 = \langle \psi_1 | i[H_d, H_p] | \psi_1 \rangle = \sum_{j=1}^N \alpha_j \langle \psi_1 | P_j | \psi_1 \rangle, \quad (27)$$

where  $\alpha_j$  are scalar coefficients and  $P_j$  are Pauli basis operators. We note that the number of Pauli basis operators  $N$  in the expansion depends on the structure of  $H_p$  and  $H_d$  (see Eq. (46) below). Each  $P_j$  can then be measured, and the measurements can be repeated to collect sufficiently many samples to estimate the associated expectation values. Finally, the resultant expectation values of each  $P_j$  can then be used to evaluate the weighted sum in Eq. (27) to estimate  $A_1$ . Following this, the result is “fed back” to set  $\beta_2 = -A_1$  (or, more precisely,  $\beta_2$  is set to be the negative of the approximation of  $A_1$ ).

For subsequent steps  $k = 2, \dots, \ell$ , the same procedure is repeated: the qubits are initialized in the state  $|\psi_0\rangle$ , after which  $k$  layers are applied to obtain

$$|\psi_k\rangle = U_d(\beta_k)U_p \cdots U_d(\beta_1)U_p|\psi_0\rangle. \quad (28)$$

Then, the qubits are measured to estimate  $A_k$  using the same procedure described above, and the result is fed back to set the value of  $\beta_{k+1}$ . By design, this procedure causes  $\langle H_p \rangle$  to decrease layer-by-layer as per

$$\langle \psi_0 | H_p | \psi_0 \rangle \geq \langle \psi_1 | H_p | \psi_1 \rangle \geq \cdots \geq \langle \psi_\ell | H_p | \psi_\ell \rangle, \quad (29)$$

such that the quality of the solution to the combinatorial optimization problem monotonically improves with circuit depth. The protocol can be terminated when the value of  $\langle H_p \rangle$  converges (i.e., stops decreasing), as determined via measurements, or when a threshold number of layers  $\ell$  is reached. At that point, the set of  $\beta$  values  $\{\beta_k\}_{k=1}^\ell$  is recorded as the output.

After Algorithm 1 concludes, the set  $\{\beta_k\}_{k=1}^\ell$  can subsequently be used to prepare the state  $|\psi_\ell\rangle$  in post-processing steps as needed, e.g., in order to estimate the value of  $\langle H_p \rangle$ , by measuring  $|\psi_\ell\rangle$  and repeating the experiment enough times to ensure reliable statistics. In addition, the associated  $\ell$ -layer quantum circuit can also be implemented in order to estimate the bit string  $z = z_1 z_2 \cdots z_n$  associated with the best candidate solution to the underlying combinatorial optimization problem. This latter task can be accomplished by sampling the bit string  $z_1 z_2 \cdots z_n$  from the output distribution associated with the output state  $|\psi_\ell\rangle$ , i.e., by measuring  $z_j = \langle \psi_\ell | Z_j | \psi_\ell \rangle$  for  $j = 1, \dots, n$  and then concatenating the results to form

$$z = z_1 z_2 \cdots z_n, \quad (30)$$

where  $Z_j$  denotes the Pauli operator acting on qubit  $j$  [63]. After collecting a set of samples, the bit string associated with the best solution to the combinatorial optimization problem, i.e., the bit string  $z$  that returns the minimum value of the associated cost function  $C(z)$ , should be saved as the best approximate solution to the combinatorial optimization problem of interest.

---

**Algorithm 1** FALQON

---

```

1: set  $H_p$ ,  $H_d$ ,  $\Delta t$ ,  $\ell$ ,  $|\psi_0\rangle$ 
2: Seed the procedure
    $\beta_1 \leftarrow 0$ 
3: Initialize the qubits
    $|\psi\rangle \leftarrow |\psi_0\rangle$ 
4: Implement 1 layer
    $|\psi\rangle \leftarrow U_d(\beta_1)U_p|\psi_0\rangle$ 
5: Estimate the value of  $A_1$  by measuring the qubits in the
   state  $|\psi_1\rangle$  and repeating the experiment enough times to
   ensure reliable statistics.
6:  $\beta_2 \leftarrow -A_1$ 
7:  $k \leftarrow 1$ 
8: while  $k < \ell$  do
9:    $k \leftarrow k + 1$ 
10:  Initialize the qubits
     $|\psi\rangle \leftarrow |\psi_0\rangle$ 
11:  Implement  $k$  layers
     $|\psi_k\rangle \leftarrow U_d(\beta_k)U_p \cdots U_d(\beta_1)U_p|\psi_0\rangle$ 
12:  Estimate the value of  $A_k$  by measuring the qubits in the
    state  $|\psi_k\rangle$  and repeating the experiment enough times to
    ensure reliable statistics.
13:  $\beta_{k+1} \leftarrow -A_k$ 
14: end while
15: output  $\{\beta_k\}_{k=1}^\ell$ 

```

---

We note that FALQON has similarities to other quantum circuit parameter-setting protocols that involve “greedy”, layer-by-layer optimization, e.g., where a classical optimization routine is used to sequentially optimize quantum circuit parameters in order to minimize a cost function in a layer-wise manner [64–67]. In fact, the parameter-setting rule given in Eq. (25) corresponds to taking a step “down” in the direction of the local gradient  $\frac{d}{d\beta_k} E_p$  with a step size of  $\Delta t$ , thus suggesting that there is a natural connection between FALQON and layer-wise circuit optimization methods that proceed by gradient descent [68]. We also remark that the ADAPT-QAOA approach developed in ref. [69] has certain similarities to FALQON, e.g., it also utilizes information about  $\frac{d}{dt} \langle \psi(t) | H_p | \psi(t) \rangle$  to step forward from layer to layer. However, their stepping procedure involves selecting from a set of driver Hamiltonians, while still containing a classical optimization loop.

Having outlined FALQON, we now turn to the prospect of boosting its performance using the techniques outlined in Secs. (II A), (II B), and (II C). We begin by discussing how a reference perturbation may be introduced, as per Eq. (8) and how the framework outlined in Sec. (II A) may be adapted to the quantum device setting. As before, this can be accomplished by simply “Trotterizing” Eq. (8), and implementing a quantum circuit with the form

$$U_d(\nu_\ell)U_p \cdots U_d(\nu_1)U_p U_d(\nu_0)U_p \quad (31)$$

where  $\nu_k = \lambda_k + \beta_k$ , where  $\lambda_k$  is the value of the reference perturbation at the  $k$ -th layer and  $\beta_k$  is the value of the control parameter at the  $k$ -th layer, determined via  $\beta_k = A_{k-1}$ . Numerical illustrations showing how the

performance of FALQON can be improved with the inclusion of a reference perturbation can be found in [58]. In a similar fashion, the iterative QLC procedure discussed in Sec. II B can also be adapted the context of quantum optimization, in order to successively improve the quality of the solutions obtained. After applying a first-order Trotter decomposition, the circuits at the  $j$ -th iteration will have the structure

$$U_d(\beta_\ell^{(j)})U_p \cdots U_d(\beta_1^{(j)})U_p U_d(\beta_0^{(j)})U_p, \quad (32)$$

where  $\beta_k^{(j)} = \beta_k^{(j-1)}(t) + \tilde{\beta}_k^{(j)}(t)$  for  $k = 0, \dots, \ell$ , and the iterative procedure is seeded by determining  $\beta^{(0)}$  via Algorithm 1. Finally, the approach discussed in Sec. (II C) may also be extended to the quantum device setting, by modifying the layered quantum circuit structure to include evolutions under additional driver Hamiltonians.

### A. Selecting $\Delta t$

We now consider the selection of the time step  $\Delta t$  in order to ensure that Eq. (3) will hold. To this end, we consider a single layer of FALQON, such that

$$\begin{aligned} E_{p,t+2\Delta t} &= \langle \psi(t+2\Delta t) | H_p | \psi(t+2\Delta t) \rangle \\ &= \langle \psi(t) | e^{iH_p\Delta t} e^{iH_d\beta_t\Delta t} H_p e^{-iH_d\beta_t\Delta t} e^{-iH_p\Delta t} | \psi(t) \rangle. \end{aligned} \quad (33)$$

For the following, we adopt the notation  $\langle \cdot \rangle_t \equiv \langle \psi(t) | \cdot | \psi(t) \rangle$ . We express each of the exponentials above using a Taylor series expansion:

$$\begin{aligned} E_{p,t+2\Delta t} &= E_{p,t} + i\langle [H_d, H_p] \rangle_t \beta_t \Delta t - \langle [H_p, [H_d, H_p]] \rangle_t \beta_t \Delta t^2 \\ &\quad - \langle [H_d, [H_d, H_p]] \rangle_t \beta_t^2 \Delta t^2 + O(\Delta t^3) \\ &= E_{p,t+2\Delta t}^{(0)} + E_{p,t+2\Delta t}^{(1)} + E_{p,t+2\Delta t}^{(2)} + \dots \end{aligned} \quad (34)$$

where the superscripts label the orders of  $\Delta t$ . Since we only use  $\beta$  to design the first order term, we would like this to be the dominant term in the expansion such that

$$|E_{p,t+2\Delta t}^{(1)}| > \left| \sum_{k=2}^{\infty} E_{p,t+2\Delta t}^{(k)} \right|. \quad (35)$$

This way, designing  $E_{p,t+2\Delta t}^{(1)}$  appropriately will enforce that  $E_{p,t+2\Delta t}$  decreases. The left-side of Eq. (35) is given by

$$\begin{aligned} |E_{p,t+2\Delta t}^{(1)}| &= |\langle [H_d, H_p] \rangle_t| |\beta_t| \Delta t \\ &= |A_t| |\beta_t| \Delta t. \end{aligned} \quad (36)$$

Meanwhile, the magnitude of higher-order terms such as  $E_{p,t+2\Delta t}^{(2)}$  can be bounded as,

$$\begin{aligned} |E_{p,t+2\Delta t}^{(2)}| &= |\langle [H_p, [H_d, H_p]] \rangle_t \beta_t + \langle [H_d, [H_d, H_p]] \rangle_t \beta_t^2| \Delta t^2 \\ &\leq (|\langle [H_p, [H_d, H_p]] \rangle_t| |\beta_t|) |\beta_t| \Delta t^2 \\ &\leq (2\|H_p\| \|H_d\| + \|H_p\| \|H_d\| + \|H_d\| \|H_p\|) |\beta_t| \Delta t^2 \\ &\quad + \|H_d\| \|H_d\| + \|H_p\| \|H_d\| \\ &\quad + 2\|H_d\| \|H_d\| |\beta_t| |\beta_t| \Delta t^2 \\ &\leq (2\|H_p\|^2 \|H_d\| + 2\|H_d\|^2 \|H_p\| |\beta_t|) 2|\beta_t| \Delta t^2 \\ &= 2n_p n_d |\beta_t| (2n_p + 2n_d |\beta_t|) \Delta t^2, \end{aligned} \quad (37)$$

where in the last line we introduce the abbreviated notation  $n_d \equiv \|H_d\|$  and  $n_p \equiv \|H_p\|$ . Expressions for the magnitude of any higher-order (i.e.,  $k \geq 2$ ) term can be found following the same procedure, which results in the following general expression at  $k$ -th order:

$$|E_{p,t+2\Delta t}^{(k)}| = 2n_p n_d |\beta_t| (2n_p + 2n_d |\beta_t|)^{k-1} \Delta t^k. \quad (38)$$

Given Eq. (38), the right side of Eq. (35) can be bounded by

$$\begin{aligned} \left| \sum_{k=2}^{\infty} E_{p,t+2\Delta t}^{(k)} \right| &\leq \sum_{k=2}^{\infty} |E_{p,t+2\Delta t}^{(k)}| \\ &\leq 2n_p n_d |\beta_t| \sum_{k=2}^{\infty} (2n_p + 2n_d |\beta_t|)^{k-1} \Delta t^k \\ &= \frac{n_p n_d |\beta_t|}{n_p + n_d |\beta_t|} \left( \sum_{k=0}^{\infty} (2\Delta t(n_p + n_d |\beta_t|))^k \right. \\ &\quad \left. - 1 - 2\Delta t(n_p + n_d |\beta_t|) \right). \end{aligned} \quad (39)$$

For  $2\Delta t(n_p + n_d |\beta_t|) < 1$  the geometric series converges. Under this assumption, we can rewrite the condition in Eq. (35) as

$$\begin{aligned} |A_t| |\beta_t| \Delta t &> \frac{n_p n_d |\beta_t|}{n_p + n_d |\beta_t|} \left( \frac{1}{1 - 2\Delta t(n_p + n_d |\beta_t|)} \right. \\ &\quad \left. - 1 - 2\Delta t(n_p + n_d |\beta_t|) \right). \end{aligned} \quad (40)$$

We rearrange this equation to obtain a bound for  $\Delta t$ :

$$|\Delta t| < \frac{|A_t|}{2(2n_d n_p + |A_t|)(n_p + n_d |\beta_t|)}. \quad (41)$$

For these values of  $\Delta t$ , we can confirm that the geometric

series in Eq. (39) does converge, because

$$\begin{aligned} 1 &> 2\Delta t(n_p + n_d|\beta_t|) \\ &= \frac{2|A_t|(n_p + n_d|\beta_t|)}{2(2n_d n_p + |A_t|)(n_p + n_d|\beta_t|)} \\ &= \frac{|A_t|}{2n_d n_p + |A_t|} \end{aligned} \quad (42)$$

is always satisfied. Therefore, if  $\Delta t$  is selected according to Eq. (41), it is ensured that the QLC condition in Eq. (3) will hold, and thus, that  $E_p$  will decrease monotonically as a function of layer as desired. In practice we find that  $\Delta t$  can be chosen to be much larger than the value in Eq. (41) due to the looseness of the bound.

#### IV. APPLICATIONS TO MAXCUT

We now consider applications of FALQON towards the combinatorial optimization problem MaxCut, which aims to identify a graph partition that maximizes the number of edges that are cut. For a graph  $\mathcal{G}$ , with  $n$  nodes and edge set  $\mathcal{E}$ , the MaxCut problem Hamiltonian is defined on  $n$  qubits as

$$H_p = - \sum_{j,k \in \mathcal{E}} \frac{1}{2} (1 - w_{jk} Z_j Z_k), \quad (43)$$

where  $w_{jk}$  denote the edge weights, and for unweighted graphs,  $w_{jk} = 1$  for all  $j, k \in \mathcal{E}$ . In our analyses involving weighted graphs, we consider random edge weights  $w_{jk}$  drawn from a uniform distribution between 0 and 1. Furthermore, we consider  $H_d$  to have the standard form

$$H_d = \sum_{j=1}^n X_j. \quad (44)$$

Given these choices for  $H_p$  and  $H_d$ ,

$$\begin{aligned} A_k &= \langle \psi_k | i[H_d, H_p] | \psi_k \rangle \\ &= \sum_{j,k \in \mathcal{E}} \langle \psi_k | Y_j Z_k | \psi_k \rangle + \langle \psi_k | Z_j Y_k | \psi_k \rangle, \end{aligned} \quad (45)$$

where  $X_j$  and  $Y_j$  denote the Pauli operators acting on qubit  $j$ . As such, evaluating the feedback law  $\beta_{k+1} = -A_k = -\langle \psi_k | i[H_d, H_p] | \psi_k \rangle$  requires measuring the expectation values of

$$N \leq n(n-1) \quad (46)$$

Pauli basis operators (i.e., in this case, two-qubit Pauli strings), where the exact value of  $N$  depends on the structure of the graph under consideration.

In order to assess the performance of FALQON towards MaxCut, we consider two figures of merit: the approximation ratio,

$$r_A = \frac{\langle H_p \rangle}{\langle H_p \rangle_{\min}}, \quad (47)$$

which is proportional to the original Lyapunov function  $E_p$ , and the “success” probability of measuring the (potentially) degenerate ground state,

$$\phi = \sum_i |\langle \psi | q_{0,i} \rangle|^2, \quad (48)$$

which gives the probability of obtaining the global minimum solution to the original combinatorial optimization problem. Each of these two figures of merit can take on values between 0 and 1, where  $r_A = \phi = 1$  corresponds to the optimal (i.e., ground state) solution.

#### A. Numerical illustrations on 3-regular graphs

We now examine the performance of FALQON towards MaxCut on 3-regular graphs via a series of numerical illustrations. We consider both weighted and unweighted 3-regular graphs with  $n \in \{8, 10, \dots, 20\}$  vertices. For graphs with  $n = 8, 10$  vertices, we consider the set of all nonisomorphic, connected 3-regular graphs. For each value of  $n = 12, \dots, 20$ , we consider a set of 50 randomly-generated nonisomorphic graphs. The qubits are initialized in the ground state of  $H_d$ , and the performance of FALQON is quantified using the mean (over the set of graphs) of  $r_A$ , and  $\phi$ . We relate the performance to two reference values:  $r_A = 0.932$ , corresponding to the highest approximation ratio that can currently be guaranteed using a classical approximation algorithm (i.e., the algorithm of Goemans and Williamson [70]), and  $\phi = 0.25$ , which implies that on average, 4 repetitions will be needed in order to obtain a sample bit string corresponding to the ground state. The results are collected in Figs. 1 and 2.

In Fig. 1, the  $r_A$  and  $\phi$  results are shown, and the associated reference values are plotted in black. The solid curves show the results for unweighted graphs, while the dotted curves of corresponding color show the results for weighted graphs. We find that FALQON performs better on unweighted graphs, given that  $r_A$  and  $\phi$  appear to converge more quickly. Nonetheless, FALQON consistently leads to monotonic convergence towards very high  $r_A$  values as a function of layer for both weighted and unweighted graphs. However, for weighted graphs, we find many instances where  $\phi$  fails to converge to 1, even for  $k \gg 1000$  layers ( $k \gg 1000$  not pictured). Meanwhile, in Fig. 2 we plot the associated values of  $\beta$ , where panels (a) and (b) collect the results for weighted and unweighted 3-regular graphs, respectively. The shading shows the associated standard deviation. In both panels, the  $\beta$  curves exhibit a very consistent shape, and the standard deviation appears to shrink with increasing  $n$ . In these illustrations, the only free parameter is the time step  $\Delta t$ , which is tuned to be as large as possible, a value we call the critical time step and denote by  $\Delta t_c$ , as long as the condition in Eq. (3) is met for all (unweighted) problem instances considered up to 1,000 layers. When  $\Delta t$  is chosen to be greater than  $\Delta t_c$ , rapid oscillations

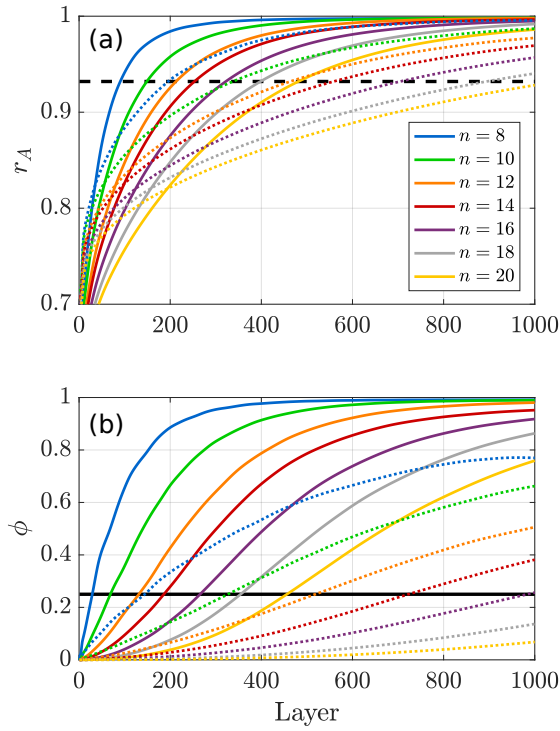


Figure 1. The performance of FALQON, as quantified by the approximation ratio  $r_A$  in (a) and the success probability  $\phi$  in (b) is shown for different values of  $n$ . The solid curves show the average results for unweighted 3-regular graphs, and the dotted curves show average results for weighted 3-regular graphs.

can form in the  $\beta$  curves, leading to a deterioration in performance (see Appendix B).

In Fig. 3, we show the performance of FALQON when it is modified using the iterative QLC heuristic introduced in Sec. II B. We apply this to a weighted instance of a 4-regular graph with  $n = 8$  vertices, where the base FALQON algorithm displays excellent convergence with respect to  $r_A$ , but where  $\phi$  fails to reach high values, and asymptotes to only  $\phi \approx 0.55$ . In Fig. 3(c), we show the  $\beta$  curves that result from three iterations of the procedure, while panel (b) shows how these iterations serve to improve the convergence of  $\phi$ .

We refer to Ref. [58] for an illustration of the improvement provided by the reference perturbation heuristic and also another random perturbation heuristic motivated by simulated annealing.

## B. Behavior under measurement noise

Here, we analyze the performance of FALQON under measurement noise, which affects each  $A_k$  value, and consequently, each  $\beta_k$  value as well. This type of noise enters due to the fact that in practice, a finite number of measurement samples  $m$  are used to estimate each  $A_k$ .

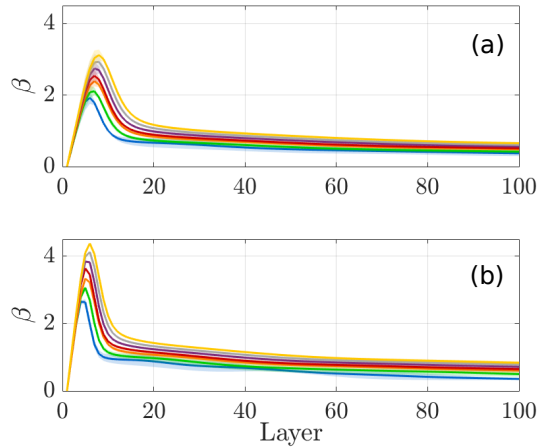


Figure 2. Mean  $\beta$  values are plotted as a function of layer, with the shading showing the corresponding standard deviations. The different colors correspond to the different values of  $n$ , as defined in the legend of Fig. 1. Panels (a) and (b) present the results for weighted and unweighted 3-regular graphs, respectively.

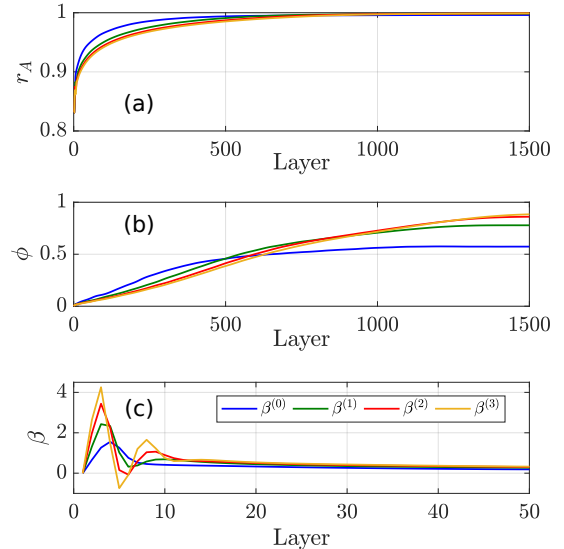


Figure 3. Performance of FALQON using the iterative QLC approach, applied to a weighted 4-regular graph,  $n = 8$ , with three iterations. In (a) and (b),  $r_A$  and  $\phi$  are plotted as a function of layer, respectively. Panel (c) shows how the associated  $\beta$  curves are refined at each iteration of the procedure.

We simulate this effect by sampling measurement outcomes from a multinomial distribution, defined at layer  $k$  as the probability distribution over the set of eigenvalues of  $i[H_d, H_p]$  when in the state  $|\psi_k\rangle$ . The results are collected in Fig. 4, which shows the performance of FALQON when  $m = 2, 5, 20$  and  $50$  samples are used to estimate  $A_k$ , for an instance of MaxCut on a 3-regular graph with 8 vertices. The results shown are representative of the behavior across other instances we studied. Our findings suggest that FALQON is robust to the ef-

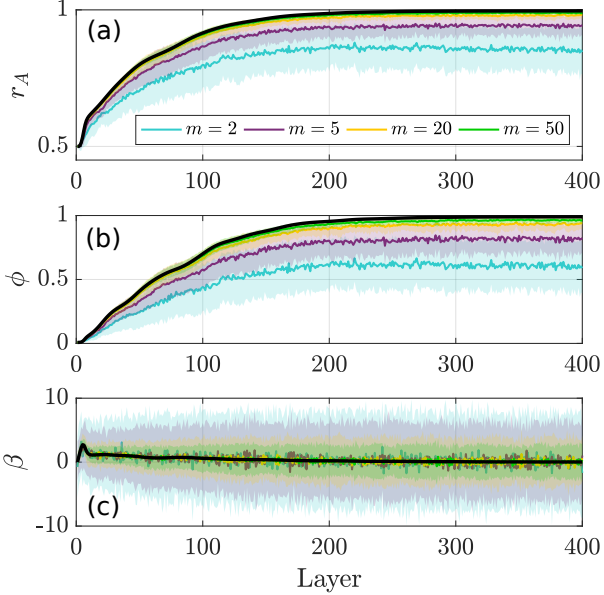


Figure 4. Performance of FALQON with  $\Delta t = 0.034$  towards an instance of MaxCut on a 3-regular graph with 8 vertices in the presence of sampling noise. In panel (a),  $r_A$  is plotted as a function of layer when  $m = 2, 5, 20$ , and 50 measurement samples are used to evaluate each  $A_k$ . The solid black curves show the ideal reference values for  $m = \infty$ , while the remaining solid curves represent the mean taken over 100 realizations of this sampling process using different  $m$  values; the shading shows the associated standard deviation. Panels (b) and (c) show analogous results for  $\phi$  and  $\beta$ , respectively.

fects of sampling noise, and can be effective even in the presence of significant measurement noise. We also find that as the number of samples  $m$  that are used decreases, performance improves if  $\Delta t$  is selected to decrease as well.

## V. COMBINING FALQON AND QAOA

As we described previously, FALQON has flexibility in the choice of a control law, e.g., Eq. (25) and the value of  $\beta_1$ , the introduction of a reference perturbation (Sec. II A), and the choice of driver Hamiltonian. Once these features are selected, FALQON is a deterministic, constructive procedure, i.e., in the limit of perfect measurements, the resulting set of parameters  $\{\beta_k\}$  is uniquely specified for a problem Hamiltonian  $H_p$ . On the other hand, QAOA has flexibility in the choice of a driver Hamiltonian(s), as well as a classical optimization method and *all* initial values of the parameter set elements  $\beta_k$  and  $\gamma_k$ .

The numerical results presented in Sec. IV suggest that solving MaxCut using FALQON alone can require many layers and therefore may not be suitable for NISQ devices with limited circuit depths. In this section, we explore how FALQON results from a smaller number of layers can be used as a seed to initialize QAOA,

thereby aiding in the subsequent search for optimal circuit parameters. Related work from Egger et al. proposes a somewhat similar idea for “warm-starting” low-depth QAOA using the solution from a relaxation of the original combinatorial optimization problem [71]. While Sack and Serbyn introduce a “Trotterized quantum annealing protocol” to initialize QAOA [72], parametrized by the time step  $\Delta t$ . In our work, we consider MaxCut on ensembles of unweighted 3-regular graphs with  $n \in \{8, 10, 12, 14\}$  vertices and 10-layer circuits implementing FALQON and QAOA. Our QAOA simulations are performed using pyQAOA [73]. As before, for graphs with  $n = 8, 10$  vertices, we consider all nonisomorphic, connected 3-regular graphs. For graphs with  $n = 12, 14$  vertices, we consider a set of 50 randomly-generated nonisomorphic graphs for each value of  $n$ .

For every graph, the set of parameters  $\{\beta_k\}$  is generated for a 10-layer circuit using FALQON as described in Algorithm 1 with  $H_d$  as specified in Eq. (44). To use the results of FALQON to initialize QAOA, the  $\beta_k$  derived from FALQON become the initial values for all  $\beta_k$  in QAOA. Analogously, all  $\gamma_k$  are initialized at  $\Delta t$  for QAOA. Within the context of the 10-layer QAOA circuit, these two sets of parameters are then optimized using a quasi-Newton optimization method (BFGS). For simplicity, we refer to this sequential FALQON + QAOA procedure as “FALQON+”. In addition, we compare the performance of FALQON+ to QAOA with random initialization, i.e., we perform QAOA using multistart BFGS with 20 randomly-selected initial values for  $\{\beta_k\}$  and  $\{\gamma_k\}$ .

Approximation ratios  $r_A$  and final-state fidelities  $\phi$  for FALQON, corresponding FALQON+, and multistart QAOA are reported in figs. 5 and 6, respectively. In both figures, the color-shaded boxes and encompassed horizontal line represent the interquartile range and the median value of the data, respectively, while the whiskers extend out to 1.5 of the interquartile range, and points beyond this range are identified as “outliers” (represented as grey diamond symbols). Comparing the results of FALQON and FALQON+, note that in addition to improved approximation ratios, FALQON+ also substantially improves the final-state fidelities, at the cost of only one application of QAOA with BFGS. Since the final state measured at the end of the circuit corresponds to an actual (approximate) solution of the MaxCut problem, increasing final-state fidelities is more important than increasing approximation ratios. For our multistart QAOA simulations, we present distributions of maximum, median, and minimum (with respect to the randomly-selected sets of initial  $\{\beta_k\}$  and  $\{\gamma_k\}$ ) approximation ratios and corresponding final-state fidelities for each ensemble of graphs. In principle, QAOA can perform better than FALQON overall since QAOA parameters can be optimized globally and QAOA parameters include the additional set  $\{\gamma_k\}$ . However, in practice, achieving this improved performance may require multiple optimizations. For our simulations, FALQON+ per-

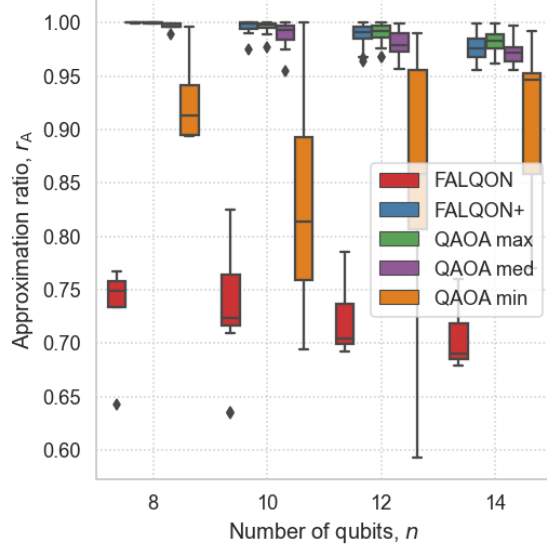


Figure 5. Performance of MaxCut on ensembles of 3-regular graphs for FALQON, FALQON+, and multistart QAOA for 10-layer circuits, quantified by the approximation ratio  $r_A$ .

forms comparably to the maximum and median cases of multistart QAOA.

In Fig. 7, we present example instances of FALQON ( $\beta_k \Delta t$  and  $\Delta t$ ) and FALQON+ ( $\beta_k$  and  $\gamma_k$ ) parameters for  $n \in \{8, 10, 12, 14\}$  vertices. Combined with Figs 5 and 6, these examples illustrate that substantial changes and improvements can occur between FALQON initialization and subsequent FALQON+ convergence, indicating that the parameters generated by FALQON, i.e.,  $\beta_k \Delta t$  and  $\Delta t$ , do not correspond to local optima for the QAOA landscape. In this sense, FALQON can prepare parameters for a successful application of QAOA, thereby reducing the expense of the optimization effort for QAOA. Although not presented here, the parameter differences presented in Fig. 7 are typical of all of our simulation results.

Based on our results and analysis, FALQON+ may provide a solution to the challenge of identifying optimal parameters for QAOA. Overall, our results demonstrate that FALQON can be used to enhance the performance of depth-limited QAOA, with minimal additional cost. See ref. [58] for estimates FALQON and QAOA sampling complexity.

## VI. QUANTUM ANNEALING APPLICATIONS

Quantum annealing [74] is an approach for preparing the ground state of a problem Hamiltonian  $H_p$  that proceeds by initializing a quantum system in the ground state of another Hamiltonian  $H_d$ , and then evolving the system via the time-dependent Hamiltonian

$$H(t) = u(t)H_d + (1 - u(t))H_p \quad (49)$$

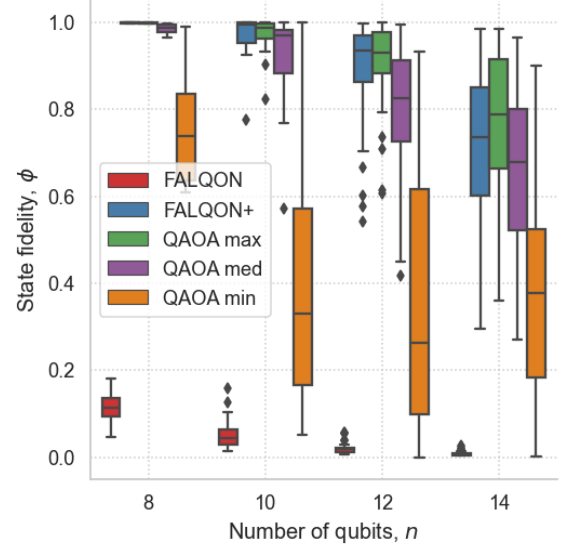


Figure 6. Performance of MaxCut on ensembles of 3-regular graphs for FALQON, FALQON+, and multistart QAOA for 10-layer circuits, quantified by the final-state fidelity  $\phi$ .

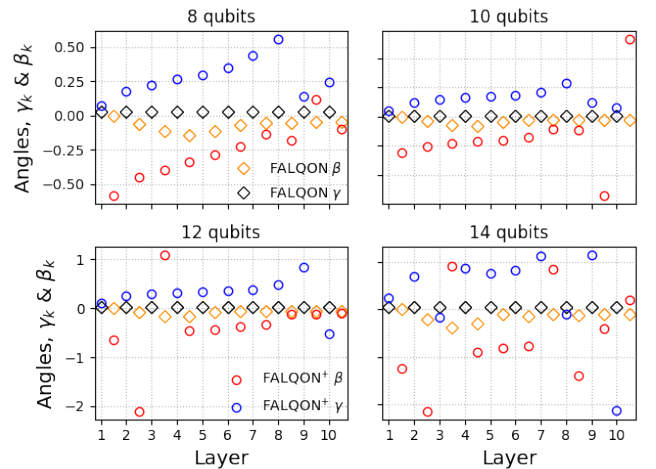


Figure 7. Comparison of FALQON and corresponding FALQON+ parameters for randomly-chosen instances of 3-regular graphs of  $n$  vertices for  $n \in \{8, 10, 12, 14\}$ . Orange and black diamonds denote FALQON  $\beta_k \Delta t$  and  $\gamma_k = \Delta t$  angles; red and blue circles denote to FALQON+  $\beta_k$  and  $\gamma_k$  angles.

for  $t \in [0, T]$ , where  $u(t)$  is the quantum annealing schedule, with  $u(0) = 1$  and  $u(T) = 0$ . Without known structure in  $H_p$  to exploit, often the simplest annealing schedule is linear, where  $u(t) = 1 - t/T$ , and we consider this in the following. Then, the aim is to choose  $T$  to be large enough such that the system remains in the instantaneous ground state of  $H(t)$  at all times, so that as  $H_p$  is slowly turned on, this will evolve the system into the ground state of  $H_p$  at time  $T$ .

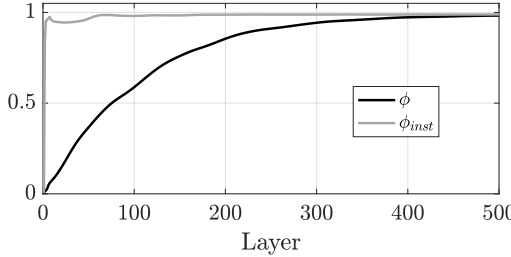


Figure 8. The ground state overlap  $\phi$  and the instantaneous ground state overlap  $\phi_{\text{inst}}$  are plotted as a function of layer, for an application of FALQON to MaxCut on an unweighted 3-regular graph with  $n = 8$  vertices. The instantaneous ground state overlap remains  $\approx 1$ , which is representative of the behavior seen across other MaxCut instances, and suggests that FALQON may proceed via an adiabatic mechanism.

In this section, we compare FALQON to linear quantum annealing because of numerical evidence suggesting that FALQON may proceed via a similar adiabatic mechanism, i.e., by slowly switching on the problem Hamiltonian  $H_p$ , such that the system remains in the instantaneous ground state. Evidence of this potential adiabatic behavior is shown in Fig. 8, for a representative instance of unweighted 3-regular MaxCut on  $n = 8$  vertices with  $\Delta t = \Delta t_c$ . The instantaneous ground state overlap  $\phi_{\text{inst}}$  is computed as  $\phi_{\text{inst}} = \sum_j |\langle \psi | \tilde{q}_{0,j} \rangle|^2$ , where the sum is taken over  $j$  degenerate instantaneous ground states (found numerically, as the eigenstates whose associated eigenvalues are within 0.01 of the lowest eigenvalue); the set of instantaneous eigenstates  $\{\tilde{q}\}$  is computed by numerically diagonalizing  $H_p + \beta H_d$  at each layer. The consistently high values of  $\phi_{\text{inst}}$  in Fig. 8 suggest that FALQON may give rise to a Trotterized version of an adiabatic process, i.e., in which strong rotations are applied initially to transfer  $|\psi\rangle$  into the instantaneous ground state, and then, the system remains primarily in the instantaneous ground state for the remaining evolution. In order to achieve this behavior, we see in Fig. 2 that  $\beta$  initially has large values, then decreases monotonically as a function of layer, similar to the behavior of an annealing schedule  $u(t)$ . Particularly notable from Fig. 2 is that the  $\beta$  curves appear to concentrate around a single average curve for each value of  $n$ , indicating that there may be a universal FALQON solution for this class of problems. As such, we relate these curves to digitized quantum annealing schedules, and consider the digitized time  $T = 2k\Delta t$  needed to achieve  $r_A = 0.932$  or  $\phi = 0.25$  using FALQON. The results are shown in Fig. 9, which shows that  $T$  scales favorably with respect to  $n$ , with a linear scaling at the problem sizes evaluated.

We then compare the performance of FALQON against that of a digitized linear quantum annealing schedule. We present the results of our numerical comparison in Fig. 10 for the same MaxCut problem instances considered in Fig. 1. Our findings indicate that for the same value of  $T$ , FALQON consistently shows stronger performance, as quantified by both  $r_A$  and  $\phi$ .

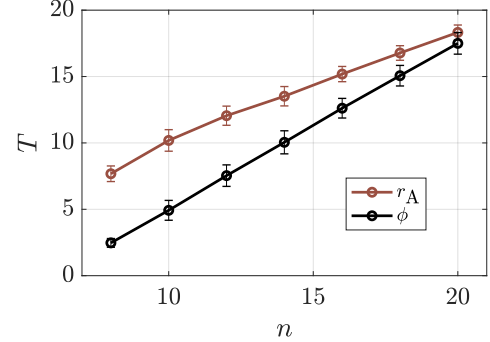


Figure 9. The mean time  $T$  needed to achieve the reference values of  $r_A = 0.932$  (dashed curve) and  $\phi = 0.25$  (solid curve) using a FALQON-inspired annealing schedule is shown.

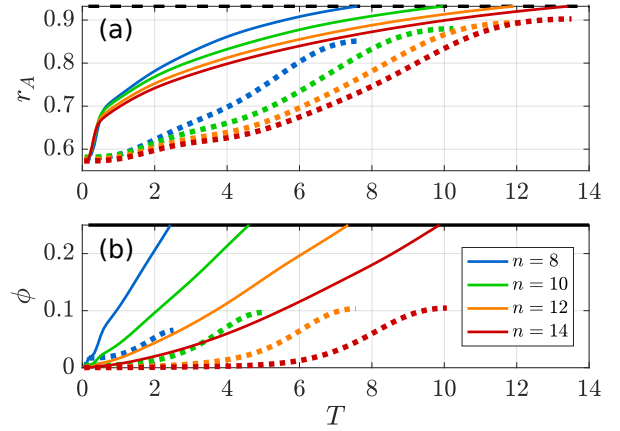


Figure 10. (a) The mean approximation ratios obtained by FALQON (solid curves) and a linear quantum annealing schedule (dotted curves) for  $n = 8, 10, 12, 14$ . For the latter, for each value of  $n$ ,  $T$  is chosen to be the time when FALQON reaches  $r_A = 0.932$ . Panel (b) shows the corresponding results for the  $\phi$ .

It is of course important to note that this comparison is limited insofar as we compare only to a linear annealing schedule. This restriction was chosen for simplicity; it remains to be seen how FALQON compares relative to quantum annealing with various optimized schedules [75–77]. Nevertheless, these results suggest that feedback-based protocols could be useful for improving performance of analog annealing devices as well. For example, the control schedule determined by FALQON,  $\beta(t)$ , could be used as the basis for an adiabatic annealing schedule. Alternatively, an annealing schedule could be derived through execution of an analogous Lyapunov-control inspired feedback strategy on an analog annealer, assuming the required measurements for determining  $A(t)$  could be performed.

## VII. OUTLOOK

We have introduced FALQON as a constructive, feedback-based algorithm for solving combinatorial optimization problems using quantum computers, and explored its utility towards the MaxCut problem via a series of numerical experiments. Crucially, FALQON does not require classical optimization, unlike other quantum optimization frameworks such as QAOA. However, this advantage comes at a cost. As we found in our numerical illustrations, the quantum circuits needed tend to be much deeper than those conventionally considered in QAOA, suggesting that there is a tradeoff between the classical and quantum costs. Furthermore, for a comparison of the sampling complexity of FALQON and QAOA, we refer the reader to [58].

Our numerical demonstrations utilized the feedback law given in Eq. (25), although a much broader class of functions could be considered, as per Eq. (6), and the performance for different choices of  $w$  and  $f$  should be explored. Furthermore, the use of bang-bang control laws, e.g., where  $\beta \in \{\pm\beta_{\max}\}$  switches between  $\pm\beta_{\max}$ , for a value of  $\beta_{\max}$  chosen according to the sign of  $A$ , could also be considered in the future. Furthermore, we remark that the performance of FALQON depends on the choice of  $\Delta t$ , suggesting that it may be possible to design methods to optimally or adaptively choose  $\Delta t$ , e.g., for a given problem, or in a layer-by-layer manner based on measurement data, perhaps informed by Eq. (41), in order to enhance the algorithm performance.

In future implementations, FALQON could be used alone as a substitute for conventional QAOA, or it could be used in combination with QAOA (e.g., by taking  $|\psi_0\rangle$  to be the terminal state from an already-optimized QAOA circuit). Similarly, in this work we have explored how FALQON could be used to seed QAOA, by identifying a set of initial QAOA parameters that can serve as the starting point for subsequent classical optimization. We expect that this seeding procedure may have particular benefit in settings with limited circuit depth, in cases where FALQON fails to converge on its own, and in cases where QAOA fails to converge on its own due to difficulty with effective initialization of the classical optimization procedure.

We further remark that in situations where circuit depth is limited, FALQON can be extended to incorporate additional driver Hamiltonians, drawing on the framework outlined in Sec. II C, and it could also be modified to use a hardware-inspired ansatz, where the circuit is formed by alternating rounds of an Ising Hamiltonian defined by the hardware connectivity, denoted as  $H_h$ , and a driver Hamiltonian  $H_d$ , while the objective remains determined by the Ising problem Hamiltonian, denoted as  $H_p$ . In this scenario, despite changes in the structure of the quantum circuits, the measurements of

$i[H_d, H_p]$  needed to assign values to the  $\beta$  parameters would remain unchanged.

Finally, we note that the feedback-based approach we have developed here can be applied to combinatorial optimization problems beyond MaxCut, *e.g.*, [78], and could have broader implications for quantum variational algorithms. It is possible to develop feedback-based alternatives of variational ansatzé for other applications such as electronic structure or machine learning [79], and these would have the benefit of needing no classical optimization resources, at the cost of requiring measurements whose results condition the feedback.

## ACKNOWLEDGMENTS

We acknowledge discussions with C. Arenz, L. Brady, L. Cincio, T.S. Ho, L. Kocia, O. Parekh, H. Rabitz, and K. Young. This work was supported by the U.S. Department of Energy, Office of Science, Office of Advanced Scientific Computing Research, under the Quantum Computing Application Teams program. A.B.M. also acknowledges support from the U.S. Department of Energy, Office of Science, Office of Advanced Scientific Computing Research, Department of Energy Computational Science Graduate Fellowship under Award Number DE-FG02-97ER25308. M.D.G. also acknowledges support from the U.S. Department of Energy, Office of Advanced Scientific Computing Research, under the Quantum Algorithm Teams program. SAND2021-9870 O.

Sandia National Laboratories is a multimission laboratory managed and operated by National Technology & Engineering Solutions of Sandia, LLC, a wholly owned subsidiary of Honeywell International Inc., for the U.S. Department of Energy's National Nuclear Security Administration under contract DE-NA0003525. This paper describes objective technical results and analysis. Any subjective views or opinions that might be expressed in the paper do not necessarily represent the views of the U.S. Department of Energy or the United States Government.

This report was prepared as an account of work sponsored by an agency of the United States Government. Neither the United States Government nor any agency thereof, nor any of their employees, makes any warranty, express or implied, or assumes any legal liability or responsibility for the accuracy, completeness, or usefulness of any information, apparatus, product, or process disclosed, or represents that its use would not infringe privately owned rights. Reference herein to any specific commercial product, process, or service by trade name, trademark, manufacturer, or otherwise does not necessarily constitute or imply its endorsement, recommendation, or favoring by the United States Government or any agency thereof. The views and opinions of authors expressed herein do not necessarily state or reflect those of the United States Government or any agency thereof.

[1] A. B. Finnila, M. Gomez, C. Sebenik, C. Stenson, and J. D. Doll, *Chem. Phys. Lett.* **219**, 343 (1994).

[2] T. Kadowaki and H. Nishimori, *Phys. Rev. E* **58**, 5355 (1998).

[3] J. Brooke, D. Bitko, G. Aeppli, *et al.*, *Science* **284**, 779 (1999).

[4] C. Durr and P. Hoyer, “A quantum algorithm for finding the minimum,” (1996), arXiv:9607014 [quant-ph].

[5] C. Dürr, M. Heiligman, P. Hoyer, and M. Mhalla, *SIAM J. Comput.* **35**, 1310 (2006).

[6] E. Farhi, J. Goldstone, and S. Gutmann, “A Quantum Approximate Optimization Algorithm,” (2014), arXiv:1411.4028 [quant-ph].

[7] J. Otterbach, R. Manenti, N. Alidoust, A. Bestwick, M. Block, B. Bloom, S. Caldwell, N. Didier, E. S. Fried, S. Hong, *et al.*, “Unsupervised machine learning on a hybrid quantum computer,” (2017), arXiv:1712.05771 [quant-ph].

[8] M. Willsch, D. Willsch, F. Jin, H. De Raedt, and K. Michielsen, *Quantum Inf. Process.* **19**, 197 (2020).

[9] D. M. Abrams, N. Didier, B. R. Johnson, M. P. da Silva, and C. A. Ryan, *Nat. Electron.* **3**, 744 (2020).

[10] A. Bengtsson, P. Vikstål, C. Warren, M. Svensson, X. Gu, A. F. Kockum, P. Krantz, C. Križan, D. Shiri, I.-M. Svensson, G. Tancredi, G. Johansson, P. Delsing, G. Ferrini, and J. Bylander, *Phys. Rev. Applied* **14**, 034010 (2020).

[11] M. P. Harrigan, K. J. Sung, M. Neeley, K. J. Satzinger, F. Arute, K. Arya, J. Atalaya, J. C. Bardin, R. Barends, S. Boixo, and *et al.*, *Nat. Phys.* **17**, 332 (2021).

[12] G. Pagano, A. Bapat, P. Becker, K. S. Collins, A. De, P. W. Hess, H. B. Kaplan, A. Kyriyanidis, W. L. Tan, C. Baldwin, and *et al.*, *Proc. Natl. Acad. Sci. U.S.A* **117**, 25396 (2020).

[13] J. Preskill, *Quantum* **2**, 79 (2018).

[14] A. B. Magann, C. Arenz, M. D. Grace, T.-S. Ho, R. L. Kosut, J. R. McClean, H. A. Rabitz, and M. Sarovar, *PRX Quantum* **2**, 010101 (2021).

[15] C. Brif, R. Chakrabarti, and H. Rabitz, *New J. Phys.* **12**, 075008 (2010).

[16] S. J. Glaser, U. Boscain, T. Calarco, C. P. Koch, W. Köckenberger, R. Kosloff, I. Kuprov, B. Luy, S. Schirmer, T. Schulte-Herbrüggen, D. Sugny, and F. K. Wilhelm, *Eur. Phys. J. D* **69**, 279 (2015).

[17] C. Altafini, *J. Math. Phys.* **43**, 2051 (2002).

[18] F. Albertini and D. D’Alessandro, *Linear Algebra Appl.* **350**, 213 (2002).

[19] S. G. Schirmer, H. Fu, and A. I. Solomon, *Phys. Rev. A* **63**, 063410 (2001).

[20] H. Fu, S. G. Schirmer, and A. I. Solomon, *J. Phys. A* **34**, 1679 (2001).

[21] G. Turinici and H. Rabitz, *J. Phys. A* **36**, 2565 (2003).

[22] D. Burgarth, D. D’Alessandro, L. Hogben, S. Severini, and M. Young, *IEEE Trans. Automat. Contr.* **58**, 2349 (2013).

[23] C. Arenz, D. Burgarth, P. Facchi, V. Giovannetti, H. Nakazato, S. Pascazio, and K. Yuasa, *Phys. Rev. A* **93**, 062308 (2016).

[24] C. Arenz and H. Rabitz, *Phys. Rev. Lett.* **120**, 220503 (2018).

[25] S. Lloyd, “Quantum approximate optimization is computationally universal,” (2018), arXiv:1812.11075 [quant-ph].

[26] M. E. Morales, J. Biamonte, and Z. Zimborás, *Quantum Inf. Process.* **19**, 1 (2020).

[27] G. Bigan Mbeng, R. Fazio, and G. Santoro, “Quantum Annealing: a journey through Digitalization, Control, and hybrid Quantum Variational schemes,” (2019), arXiv:1906.08948 [quant-ph].

[28] Z.-C. Yang, A. Rahmani, A. Shabani, H. Neven, and C. Chamon, *Phys. Rev. X* **7**, 021027 (2017).

[29] A. Bapat and S. Jordan, *Quantum Inf. Comput.* **19**, 424 (2019).

[30] L. T. Brady, C. L. Baldwin, A. Bapat, Y. Kharkov, and A. V. Gorshkov, *Phys. Rev. Lett.* **126**, 070505 (2021).

[31] A. S. Berahas, R. H. Byrd, and J. Nocedal, *SIAM J. Optim.* **29**, 965 (2019).

[32] R. Chakrabarti and H. Rabitz, *Int. Rev. Phys. Chem.* **26**, 671 (2007).

[33] B. Russell, H. Rabitz, and R.-B. Wu, *J. Phys. A* **50**, 205302 (2017).

[34] J. R. McClean, S. Boixo, V. N. Smelyanskiy, R. Babbush, and H. Neven, *Nat. Commun.* **9**, 1 (2018).

[35] C. Arenz and H. Rabitz, *Phys. Rev. A* **102**, 042207 (2020).

[36] R. Wiersema, C. Zhou, Y. de Sereville, J. F. Carrasquilla, Y. B. Kim, and H. Yuen, *PRX Quantum* **1**, 020319 (2020).

[37] L. Bittel and M. Kliesch, “Training variational quantum algorithms is NP-hard – even for logarithmically many qubits and free fermionic systems,” (2021), arXiv:2101.07267 [quant-ph].

[38] J. Lee, A. B. Magann, H. A. Rabitz, and C. Arenz, “Towards favorable landscapes in quantum combinatorial optimization,” (2021), arXiv:2105.01114 [quant-ph].

[39] M. Larocca, P. Czarnik, K. Sharma, G. Muraleedharan, P. J. Coles, and M. Cerezo, “Diagnosing barren plateaus with tools from quantum optimal control,” (2021), arXiv:2105.14377 [quant-ph].

[40] P. Gross, H. Singh, H. Rabitz, K. Mease, and G. M. Huang, *Phys. Rev. A* **47**, 4593 (1993).

[41] Y. Chen, P. Gross, V. Ramakrishna, H. Rabitz, and K. Mease, *J. Chem. Phys.* **102** (1995).

[42] A. G. Campos, D. I. Bondar, R. Cabrera, and H. A. Rabitz, *Phys. Rev. Lett.* **118**, 083201 (2017).

[43] G. McCaul, C. Orthodoxou, K. Jacobs, G. H. Booth, and D. I. Bondar, *Phys. Rev. A* **101**, 053408 (2020).

[44] G. McCaul, C. Orthodoxou, K. Jacobs, G. H. Booth, and D. I. Bondar, *Phys. Rev. Lett.* **124**, 183201 (2020).

[45] R. Kosloff, A. D. Hammerich, and D. Tannor, *Phys. Rev. Lett.* **69**, 2172 (1992).

[46] M. Sugawara and Y. Fujimura, *J. Chem. Phys.* **100**, 5646 (1994).

[47] M. Sugawara and Y. Fujimura, *Chem. Phys.* **196**, 113 (1995).

[48] Y. Ohtsuki, Y. Yahata, H. Kono, and Y. Fujimura, *Chem. Phys. Lett.* **287**, 627 (1998).

[49] D. J. Tannor, R. Kosloff, and A. Bartana, *Faraday Discuss.* **113**, 365 (1999).

[50] M. Sugawara, *J. Chem. Phys.* **118**, 6784 (2003).

[51] S. Grivopoulos and B. Bamieh, in *42nd IEEE International Conference on Decision and Control (IEEE Cat.*

*No.03CH37475*), Vol. 1 (2003) pp. 434–438 Vol.1.

[52] M. Mirrahimi, G. Turinici, and P. Rouchon, *J. Phys. Chem. A* **109** *11*, 2631 (2005).

[53] V. Engel, C. Meier, and D. J. Tannor, “Local control theory: Recent applications to energy and particle transfer processes in molecules,” in *Advances in Chemical Physics* (John Wiley & Sons, Ltd, 2009) pp. 29–101.

[54] A. C. Doherty, S. Habib, K. Jacobs, H. Mabuchi, and S. M. Tan, *Phys. Rev. A* **62**, 012105 (2000).

[55] H. M. Wiseman and G. J. Milburn, *Quantum measurement and control* (Cambridge University Press, 2009).

[56] J. Combes, J. Kerckhoff, and M. Sarovar, *Adv. Phys.: X* **2**, 784 (2017).

[57] J. Zhang, Y.-x. Liu, R.-B. Wu, K. Jacobs, and F. Nori, *Phys. Rep.* **679**, 1 (2017).

[58] A. B. Magann, K. M. Rudinger, M. D. Grace, and M. Sarovar, “Feedback-based quantum optimization,” (2021), arXiv:2103.08619 [quant-ph].

[59] A. Isidori, M. Thoma, E. D. Sontag, B. W. Dickinson, A. Fettweis, J. L. Massey, and J. W. Modestino, *Nonlinear Control Systems*, 3rd ed. (Springer-Verlag, Berlin, Heidelberg, 1995).

[60] S. Cong and F. Meng, *Sci. World J.* **2013** (2013).

[61] K. Beauchard, J. M. Coron, M. Mirrahimi, and P. Rouchon, *Syst. Control. Lett.* **56**, 388 (2007).

[62] S. Zhao, H. Lin, J. Sun, and Z. Xue, *Int. J. Robust Nonlinear Control* **22**, 1212 (2012).

[63] For applications of FALQON to MaxCut on regular graphs, as studied in Sec. IV, the results of this procedure for measuring the bit string  $z_1 z_2 \cdots z_n$  will be concentrated around the mean when shallow circuits are used. The proof for concentration of  $\langle H_p \rangle$  for fixed  $\ell$  follows directly from the proof in Sec. III of [6]. Given that  $H_p$  and  $Z_1 Z_2 \cdots Z_n$  are both diagonal in the measured, computational basis, it follows that concentration holds for the latter as well.

[64] J. Carolan, M. Mohseni, J. P. Olson, M. Prabhu, C. Chen, D. Bunandar, M. Y. Niu, N. C. Harris, F. N. Wong, M. Hochberg, *et al.*, *Nat. Phys.* **16**, 322 (2020).

[65] A. Skolik, J. R. McClean, M. Mohseni, P. van der Smagt, and M. Leib, *Quantum Mach. Intell.* **3**, 1 (2021).

[66] E. Campos, A. Nasrallah, and J. Biamonte, *Phys. Rev. A* **103**, 032607 (2021).

[67] E. Campos, D. Rabinovich, V. Akshay, and J. Biamonte, “Training saturation in layerwise quantum approximate optimisation,” (2021), arXiv:2106.13814 [quant-ph].

[68] G. Verdon, J. M. Arrazola, K. Brádler, and N. Killoran, “A quantum approximate optimization algorithm for continuous problems,” (2019), arXiv:1902.00409 [quant-ph].

[69] L. Zhu, H. L. Tang, G. S. Barron, N. J. Mayhall, E. Barnes, and S. E. Economou, “An adaptive quantum approximate optimization algorithm for solving combinatorial problems on a quantum computer,” (2020), arXiv:2005.10258 [quant-ph].

[70] M. X. Goemans and D. P. Williamson, *J. ACM* **42**, 1115 (1995).

[71] D. J. Egger, J. Marecek, and S. Woerner, “Warm-starting quantum optimization,” (2021), arXiv:2009.10095 [quant-ph].

[72] S. H. Sack and M. Serbyn, “Quantum annealing initialization of the quantum approximate optimization algorithm,” (2021), arXiv:2101.05742 [quant-ph].

[73] G. von Winckel, “pyQAOA: Simulation of Quantum Approximate Optimization Algorithms in Python,” <https://github.com/gregvw/pyQAOA> (2021), accessed: 2021-07-27.

[74] A. Das and B. K. Chakrabarti, *Rev. Mod. Phys.* **80**, 1061 (2008).

[75] J. Roland and N. J. Cerf, *Phys. Rev. A* **65**, 042308 (2002).

[76] C. Brif, M. D. Grace, M. Sarovar, and K. C. Young, *New J. Phys.* **16**, 065013 (2014).

[77] L. Zeng, J. Zhang, and M. Sarovar, *J. Phys. A* **49**, 1 (2016).

[78] D. Wakeham and J. Ceroni, “Feedback-Based Quantum Optimization (FALQON),” [https://pennylane.ai/qml/demos/tutorial\\_falqon.html](https://pennylane.ai/qml/demos/tutorial_falqon.html) (2021), accessed: 2021-05-21.

[79] M. Cerezo, A. Arrasmith, R. Babbush, S. C. Benjamin, S. Endo, K. Fujii, J. R. McClean, K. Mitarai, X. Yuan, L. Cincio, and et al., “Variational quantum algorithms,” (2020), arXiv:2012.09265 [quant-ph].

[80] J. P. La Salle, *The stability of dynamical systems* (SIAM, 1976).

## Appendix A: Convergence of QLC

Within the QLC framework outlined in Sec. II, it has been shown that asymptotic convergence to the ground state of  $H_p$  can be guaranteed when the following sufficient criteria are met [51, 60–62]:

1.  $H_p$  has no degenerate eigenvalues, i.e.,  $q_i \neq q_j$  for  $i \neq j$  where  $q_i$  and  $q_j$  are the  $i$ -th and  $j$ -th eigenvalues of  $H_p$
2.  $H_p$  has no degenerate eigenvalue gaps, i.e.,  $\omega_{ji} \neq \omega_{lk}$  for  $(i, j) \neq (k, l)$ , where  $\omega_{ji} = q_j - q_i$  is the gap between the  $i$ -th and  $j$ -th eigenvalues of  $H_p$
3.  $\langle q_j | H_d | q_i \rangle \neq 0$  for all  $i \neq j$
4.  $E_p(|q_0\rangle) < E_p(|\psi(t=0)\rangle) < E_p(|q_1\rangle)$

In particular, if criteria 1-3 are met, then the LaSalle invariance principle [80] can be used to show that any initial state  $|\psi(t=0)\rangle$  will converge asymptotically to the largest invariant set, i.e., the largest set of states where  $\frac{d}{dt}E_p = 0$ . When  $E_p$  is chosen per Eq. (2), it can be shown that the largest invariant set is the set of eigenstates of  $H_p$ . Within this set, the eigenstate  $|q_0\rangle$  with the smallest eigenvalue is the minimum, the eigenstate with the largest eigenvalue is the maximum, and all

other eigenstates with intermediate eigenvalues are saddle points. In order to ensure convergence to the desired critical point  $|q_0\rangle$ , criterion (4) stipulates that the value of  $E_p(|\psi(0)\rangle)$  at time  $t = 0$  must be strictly lower than  $E_p(|q_1\rangle) = q_1$ , such that the only critical point inside  $E_p(|\psi(t)\rangle) \leq E_p(|\psi(0)\rangle)$  is the desired target,  $|q_0\rangle$ . Thus, the satisfaction of criteria (1)-(4) is sufficient to ensure that the system state will converge asymptotically to the desired target  $|q_0\rangle$  [51, 60–62].

## Appendix B: Selecting $\Delta t > \Delta t_c$

Fig. 11 illustrates the effects of selecting a time step that is too large, i.e.,  $\Delta t > \Delta t_c$ , for an instance of unweighted, 3-regular MaxCut on  $n = 8$  vertices, with  $\Delta t = 0.065$ . The behavior in Fig. 11 is representative of the behavior seen across other instances when  $\Delta t > \Delta t_c$ . In general, there is a balance between selecting a large  $\Delta t$  for improving convergence *and* satisfying  $\Delta t \leq \Delta t_c$  for ensuring monotonic improvement in  $E_p$ .

## Appendix C: Log-log plot of MaxCut results

In Fig. 12, we plot the results presented in the main text in Fig. 1 using a log-log scale.

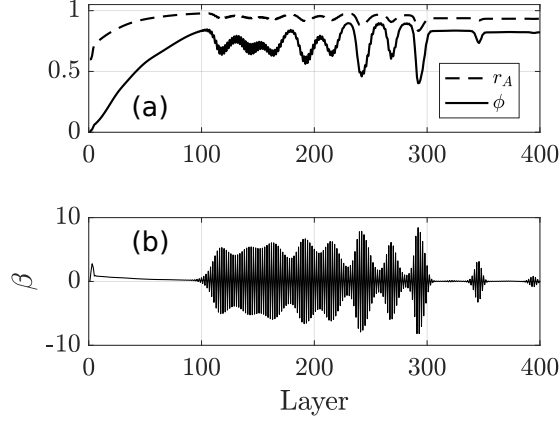


Figure 11. Typical behavior when  $\Delta t$  is chosen to be too large, leading to a violation of the QLC criterion that  $\langle H_p \rangle$  decreases monotonically with respect to circuit depth. In (a), the behavior of  $r_A$  and  $\phi$  are shown, with the violation in monotonicity occurring around 100 layers. In (b), the associated behavior of  $\beta$  is plotted, indicating that the violation of the QLC criterion corresponds to the creation of rapid oscillations in  $\beta$ .

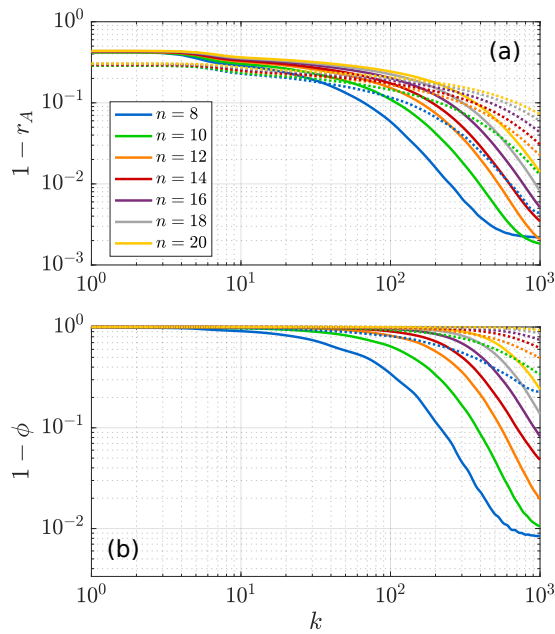


Figure 12. The performance of FALQON, as quantified by the approximation ratio  $r_A$  in (a) and the success probability  $\phi$  in (b), is shown as a function of the layer  $k$  for different values of  $n$  on a log-log scale. The same results are plotted on a linear scale in Fig. 1. The solid curves show the average results for unweighted 3-regular graphs, and the dotted curves show average results for weighted 3-regular graphs.